SGG SGS sc | nat
Swiss Journal of Geosciences

RESEARCH Open Access

Characterization of the 1584 Corbeyrier and Yvorne "Ovaille" mass movement deposits by multimethod geophysical surveying and drilling

Ariane Maharaj[1*], György Hetényi[1], James Irving[1], Valerio Poggi[2], Daniel Kurzen[1], Yanis Fernandez[1] and Jean-Luc Epard[1]

Abstract

The Corbeyrier and Yvorne mass movement events that happened in the year 1584 have mainly been studied at the surface level such that the shallow subsurface structure remains largely unknown. Geophysical measurements allow for insights into the physical properties of the subsurface including the geometry of deposits after such events. We applied three methods with the specific interest of obtaining information about the spatial variation of thickness and lithology of the mass movement deposits: the horizontal to vertical spectral ratio of ambient seismic noise (54 measurements), electrical resistivity tomography (2 profiles) and ground-penetrating radar (7 profiles). These measurements were then complemented with a physical sample obtained from drilling a 10.6 m long core in the Luan forest. We found that the mass movement deposits contain angular clasts of gravel and cobbles in a clay matrix (~ 30%). We also saw a thinning of the deposits downslope such that they reached a thickness of 3.5 m in the Luan forest and a thickness greater than 10 m (estimated between 50 and 100 m) near the source region at Plan Falcon. We identified two areas which call for further investigation in terms of the possibility of sediment mobility of the deposits in the event of an earthquake: Plan Falcon and the mostly bare scree slope just below.

Keywords Landslide, Horizontal to vertical spectral ratio, Ambient seismic noise, Electrical resistivity tomography, Ground penetrating radar, Drill core

1 Introduction

Mountainous regions are naturally prone to mass movements, and such events have affected or currently affect at least 6–8% of Switzerland (Raetzo & Loup, 2016). Weather and climate play a major role in the dynamics and eventual triggering of these events as seen in the recent Brienz/Brinzauls rockslide of 2023 (e.g., Häusler et al., 2025; Loew et al., 2025) and the Blatten landslide of May 2025. To a lesser extent, these events can be seismically induced with the example of the 1946 Rawilhorn rockslide/rock avalanche (5 million m^3 of material) which was triggered by a moment magnitude 5.5 aftershock four months after the magnitude 5.8 mainshock in Sierre; it was the largest of 88 mass movement events triggered by these earthquakes (e.g., Fritsche & Fäh, 2009; Moore et al., 2012). Historically, there are several records of seismically induced events that have occurred in the Alps such as in 1348, when six rockslides on the Dobratsch Mountains, Austria, were triggered by an earthquake with an

Handling editor: Simon Löw, Daniel Marty

*Correspondence:
Ariane Maharaj
ariane.maharaj@unil.ch
[1] Institute of Earth Sciences, University of Lausanne, 1015 Lausanne, Switzerland
[2] National Institute of Oceanography and Applied Geophysics, Seismological Research Center, Udine, Italy

estimated magnitude of ~ 7 mobilizing 100 million m^3 of material (e.g. Jemec Auflič et al., 2017; Caracciolo et al., 2021). Similarly, in Switzerland and the focus of this study, two mass movement events occurred in Corbeyrier and Yvorne in the canton of Vaud over four centuries ago. On the 11th of March 1584, a magnitude 5.9 earthquake (max. intensity VIII) in the region of Aigle triggered a rockfall (free fall, bouncing and rolling of individual rock blocks) in the upper flank of the Tour d'Aï mountain's south-western side. In the following days, heavy precipitation prevailed and on the 14th of March 1584 a magnitude 5.4 aftershock (max. intensity VII) led to a debris flow (rapid, concentrated flow of debris in a channel). This event brought material down to the bottom of the valley, almost entirely destroying the village of Corbeyrier, and partly covering the village of Yvorne, taking over 300 lives and causing substantial damage. Both the geological process and the consequences are described in detail in historical records and recent compilations, and for details we refer to Jeannet (1912–1918), Alexander (1983), Gisler et al. (2008), Fritsche et al. (2012), Schwarz-Zanetti et al. (2018). The catastrophic event itself and the trace of these mass movement events are locally known as the "Ovaille" (or "Orvaille") and is referred to as such hereafter. The geologically mapped trace of the Ovaille is ~ 5 km in length and extends from an elevation of 400–1500 m above sea-level (Fig. 1). Previous studies of the Ovaille have primarily focused on its surface-level geological and geographical features, with no examination of its subsurface structure (e.g. Jeannet, 1912–1918; Badoux et al., 1960; Badoux, 1965; Alexander, 1983). Therefore, the volume, lithological nature, spatial variability, and physical properties of the mass movement deposits are mostly unknown. Motivated by these questions, we investigated the thickness and heterogeneity of the Ovaille deposit layer, and the depth of the landslide slip surface, as well as gained insights into the resonance frequency and related local ground motion amplification effects in the event of an earthquake in the region.

Mass movement deposits can have very complex geometries and compositions, so in order to characterize the Ovaille deposits, we employed four methods of investigation. The first was passive seismic measurements at individual sites, the continuous recordings of which have served to calculate the horizontal to vertical spectral ratio (HVSR) of ambient seismic noise. This method effectively identifies the fundamental resonance frequency of S-waves and serves as a first-order tool for assessing major seismic impedance contrasts at depth, which can be indicative of ground amplification effects, particularly in soft sedimentary deposits overlying bedrock (e.g., Nakamura, 1989; Bard, 1999; SESAME Project, 2004; Molnar et al., 2018). The use of HVSR in mass movement studies has increased in recent years targeting the depth to the slip surface, the heterogeneity of the material, and vibrational behaviour of unstable areas (e.g. Pazzi et al., 2017; Imposa et al., 2017; Iannucci et al., 2020; Seitone et al., 2025). The HVSR method is both fast and effective, requiring only short-duration recordings to yield reliable results, depending on the lowest frequency of interest. This efficiency enabled us to perform a large number of measurements across the study area, both within and outside the Ovaille; the most detailed spatial assessment (~ 100 m scale) of subsurface variations performed on the Ovaille to date. We also conducted geophysical surveys along profile lines, specifically electrical resistivity tomography (ERT) and ground-penetrating radar (GPR) which are used extensively in subsurface imaging and have been successful in characterizing mass movement deposits and its evolution through the identification of heterogeneity and contrasts in lithology and water content, determining the thickness and structure of the material, and locating slip surfaces (e.g. Sass et al., 2008; Bichler et al., 2004; Perrone et al., 2014). These techniques allowed us to add greater perspective to the HVSR measurements by continuous imaging at approximately a 1 m scale, and to help in constraining the thicknesses of the subsurface layers and their spatial variability. Geophysical surveying is a cost-effective and non-invasive way of characterizing these types of deposits on a large spatial scale but in order to obtain ground truth, and compare and calibrate the geophysical results, a fully cored borehole was drilled. This local but valuable observation allowed us to better interpret the geophysical results, to verify the true thickness of the Ovaille deposits, and to assess the type of material deposited by the mass movements as well as the nature of underlying layer in this region. We conclude on the general characteristics of the Ovaille deposits, with a focus on the analysis of the Plan Falcon area and the loose debris (or scree) slope exposed at the surface.

1.1 Geological setting

The Ovaille was formed by the collapse of the wall overlooking the Luan cirque, eroded into the heart of the Tour d'Aï anticline, part of the Préalpes Médianes Plastiques. The sedimentary series extends from the Triassic to the Upper Jurassic (Fig. 1), according to the geological maps of Monthey and Montreux (Badoux et al., 1960; Badoux, 1965) and the work of Jeannet (1912–1918). Upper Triassic (Norian) cargneules and dolomites can be identified, forming the core of the anticline and outcropping sporadically beneath the Ovaille deposits in the bed of the Yvorne torrent, downstream from Corbeyrier. The wall overlooking Luan consists mainly of the Rhaetian and Hettangian series. These are alternating layers of

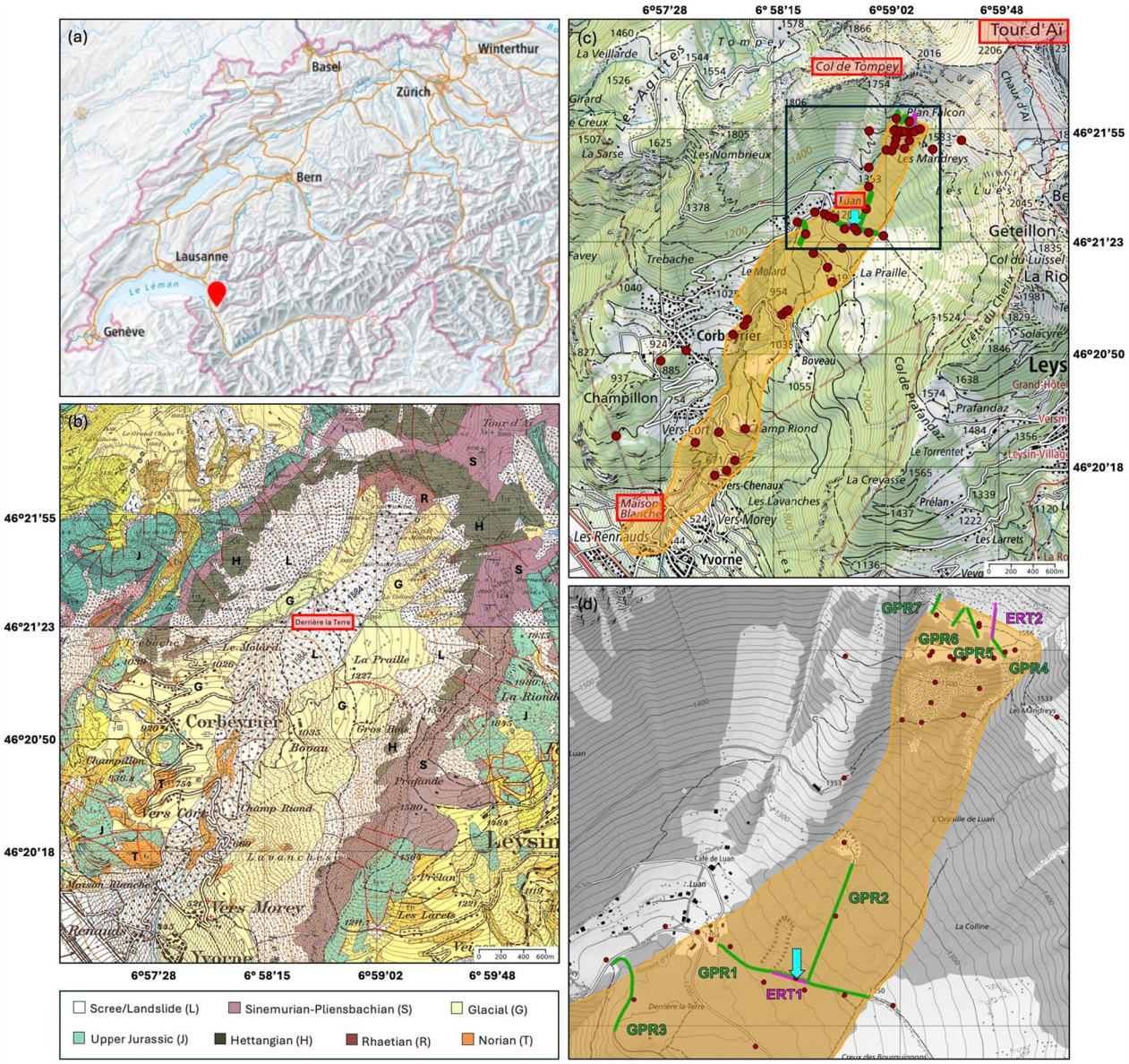

Fig. 1 **a** Map of Switzerland showing the location of the study area with a red marker. **b** Geological map of the study area. **c** Topographic map showing the locations of the seismic stations (red dots), electrical resistivity tomography (ERT) and ground penetrating radar (GPR) profiles (purple and green respectively) and the location of the drill site (blue arrow). The geologically mapped trace of the Ovaille is highlighted in orange and the black box locates the region shown in **d** which focuses on the ERT and GPR profiles. Places names mentioned in the text are highlighted in red. Basemaps and the Ovaille trace are from ©swisstopo

marl and limestone, the latter rarely exceeding one metre in thickness. The upper part of the Hettangian formations forms a hundred-metre-high escarpment, visible below the point marked 2016 (Col de Tompey). These are light-coloured cherty limestones, the only formation massive enough to generate blocks measuring several metres, such as those found in the Ovaille deposits at an elevation of around 1200 m, at "Derrière la Terre." The ridge separating Luan from the Tour d'Aï massif is formed by a well-bedded series of Sinemurian marls and argillaceous limestones. It should be noted that the massive limestones of the Upper Jurassic, which form the backbone of the Tour d'Aï anticline, are not involved in the source material of the Ovaille deposit.

The Ovaille was deposited on Quaternary glacial deposits, mainly morainic, left by the Rhône glacier and local glaciers. The distinction between the two types of moraines is difficult, as Badoux et al. (1960) points out,

since elements of gneiss, for example, clearly associated with the Rhône glacier, may have been reworked by local glaciers. In the downstream section, after flowing through the valley carved out by the Yvorne torrent, the Ovaille spreads out over an alluvial fan previously deposited by the same torrent. The thickness of the Ovaille deposit is difficult to estimate based on purely morphological criteria. Three hydrological excavations spread across the Luan forest, reaching a maximum depth of 3 m, did not reach the base of the deposit. The size of the excavated material averages a few centimetres, with some blocks less than 30 cm. In its downstream section, towards Maison Blanche, the Ovaille deposits form a characteristic lobe that is approximately 10 m thick near Maison Blanche.

2 Methods

We employed three geophysical techniques: (1) the HVSR of ambient seismic noise, (2) ERT, and (3) GPR. We also drilled a borehole, whose location was selected based on these measurements. The positions of stations and survey lines were located by GPS, and the elevation profiles were taken from the SwissALTI3D model (©swisstopo).

2.1 HVSR of ambient seismic noise

The HVSR analysis of ambient noise is the ratio between the amplitude of the Fourier spectra of the horizontal (averaged for north–south and east–west) and vertical components of continuous seismic recordings. The HVSR method was first introduced by Nogoshi and Igarashi (1970, 1971) and further developed by Nakamura (1989) as means to extract site S-wave resonance frequency and amplification of soft sediment. The peak of the HVSR curve is due to high impedance contrasts (greater than 4; SESAME Project, 2004) between layers and has been shown to give a good estimate of the resonance frequency but not of the site amplification factor (e.g. Lanchet & Bard, 1994, 1995; Ibs-von Seht & Wohlenberg, 1999; SESAME Project, 2004; Bonnefoy-Claudet et al., 2008). Rather, it has been suggested that amplification is often underestimated by the HVSR and instead the HVSR can give a lower bound estimate (e.g. Bard, 1999; Atakan et al., 2004; Haghshenas et al., 2008). We interpret the HVSR peak amplitude as an indicator of relative subsurface material property variations, which may locally influence ground motion amplification effects during earthquakes.

Ambient vibration measurements were conducted using the Raspberry Shake RS3D, a compact seismometer that integrates three-component 4.5 Hz geophones with a 24-bit digitizer, operating at a sampling rate of 100 samples per second. A total of 54 measurement points were surveyed, including 45 within the geologically mapped extent of the Ovaille (12 of which were located in the Plan Falcon area) and 9 additional points in the surrounding regions for comparison (Fig. 1). The duration of the measurements varied from 1 to 4 h, however there were disruptions with a few of the data acquisitions (possibly linked to the external GPS antenna) so continuous recordings were processed between 20-min and 4-h durations.

HVSR analysis of the ambient noise recordings was performed using the Geopsy software, (version 3.5.2; Wathelet et al., 2020) with the following settings: (a) the squared average for merging the horizontal components; (b) a Tukey window taper at 10%; (c) log–log Konno–Omachi smoothing with a *b*-value (bandwidth coefficient) of 40; and (d) non-overlapping time windows ranging from 20 to 60 s, depending on the duration of the recorded data. The selected window lengths ensured the extraction of a sufficient number of spectra for robust statistical analysis of the HVSR results, in accordance with the SESAME Project (2004) recommendations, i.e., the number of significant cycles of the predominant frequency contained in each window was always greater than 200.

The geophones integrated into the Raspberry Shakes have a natural frequency of 4.5 Hz, and a usable bandwidth ranging from 0.7 to 39 Hz. However, we processed the data with a lower frequency limit of 2 Hz as we observed increased distortion below this frequency resulting in larger standard deviations in the spectral ratios. We attribute this behaviour to a combination of factors including significant subsurface heterogeneities at greater depths where longer wavelengths penetrate deeper. We also set an upper frequency limit of 25 Hz, as higher frequencies are more susceptible to incoherent noise, scattering effects, and local subsurface variations, which can compromise the reliability of the HVSR measurements. (e.g., Aki 1957; Molnar et al., 2022). This 2–25 Hz frequency range is appropriate for our study, as we anticipate a relatively shallow impedance contrast between the Ovaille material and the underlying glacial deposits, on the order of meters to tens of meters (see Sect. 1.1, and Alexander, 1983).

2.2 ERT

ERT operates by injecting electric current into the subsurface between one pair of electrodes and measuring the corresponding difference in electrical potential between another pair of electrodes. During an ERT survey, many of such quadripole measurements are acquired for different electrode positions along a profile line, the results of which are inverted to estimate the spatial distribution of subsurface electrical resistivity. ERT measurements were made along two profiles: ERT1 in the Luan

forest, across the middle of the mapped Ovaille deposits' east–west extent, along a forest road, and ERT2 at Plan Falcon along the landslide's presumed movement direction, with the aim of mapping the contact between the deposits and the underlying layer (Fig. 1). We used a Syscal Switch Pro 96-channel resistivity meter manufactured by IRIS Instruments. The electrode spacing along each profile was 1 m, yielding a profile length of 95 m. This corresponds to an approximate depth of investigation of 15–20 m, which is within the range of the expected thickness of the mass movement deposit at least in the Luan forest. Data were acquired using both the Wenner-Schlumberger and dipole–dipole electrode configurations; the former typically better resolves vertical layering, and the latter is better suited to detecting lateral changes. A pulse duration of 500 ms and a target of 50 mV for the potential readings were set as criteria for the current injection. For each resistivity quadrupole, four repeat measurements were made to identify erroneous values and improve data quality.

Pre-processing of the ERT data was performed in MATLAB and included removing all data where the relative standard deviation of the repeat quadrupole measurements was greater than 4%, or where the measured potential was less than 5 mV. For the Wenner-Schlumberger data, this meant rejecting approximately 10% of the measurements. For the dipole–dipole data, roughly 20% of the measurements were rejected. To invert the measurements, the Boundless Electrical Resistivity Tomography (BERT) software package was used (Günther & Rücker, 2019), considering smoothness (L2-norm) prior model constraints and with inversion parameter $zweight = 0.5$ to reflect a prior model structure between isotropic ($zweight = 1$) and strongly layered ($zweight = 0.1$).

2.3 GPR

GPR operates by sending a short-duration electromagnetic impulse (MHz to GHz range) into the subsurface using a transmitter antenna. The impulse reflects off objects or interfaces across which electrical properties change, most notably the dielectric permittivity. The reflected signals are then recorded as a function of time at a receiver antenna. By acquiring GPR measurements at regular intervals along a profile line, a subsurface image can be constructed, revealing variations in electrical properties that correspond to different lithologies or changes in water content. GPR measurements were made along seven profiles. Three profiles were made in the Luan forest where the first profile, GPR1, trends roughly west to east across the Ovaille deposits overlapping with and extending further than ERT1; the second, GPR2, runs along the mass movement's flow direction perpendicular and adjacent to GPR1; and the third, GPR3, runs along another forest road which crosses the edge of the deposits. The remaining four profiles were made in Plan Falcon with GPR4 following the trend of ERT2 and extending further to the southeast, and GPR5, GPR6 and GPR7 running parallel to GPR4 on the western side of the Ovaille (Fig. 1). We used a PulseEkko Pro GPR system manufactured by Sensors & Software Inc. The transmitter and receiver antennas, having a center frequency of 100 MHz and separated by a distance of 0.5 m, were towed along each profile and GPR traces were acquired every 0.1 m using an odometer wheel trigger. Traces were recorded with a time sampling interval of 0.5 ns and a trace length of 500 ns. Each trace was stacked 10,000 times based on real-time sampling at the receiver to improve the signal-to-noise ratio of the data.

Processing of the GPR data was standard and consisted of (i) dewow, using a 31-point windowed residual median filter, to remove the low-frequency transient upon which the GPR reflection signal is superimposed; (ii) gain, using a smooth time-varying function based on the average amplitude decay curve for the dataset, to compensate for losses due to the geometrical spreading of energy and attenuation; (iii) frequency-wavenumber (f–k) migration, using the approach of Stolt (1978), to correctly image reflectors and scatterers in depth; and (iv) horizontal median filtering using an 11-point window to better highlight reflection interfaces. Migration was accomplished using a radar wave velocity for the soil of 0.1 m/ns, which was found visually to best collapse the numerous diffraction hyperbolas in the data. Note that all GPR images are presented relative to the surface topography along the survey line.

2.4 Cored drilling operation

We defined the target location of a cored borehole in the Luan forest based on several factors: the results of the ERT1 survey line, the indications from GPR1, ease of access for the drilling equipment, and constraints related to permitting. Most importantly, the ERT1 results motivated the location chosen for drilling (Fig. 1) essentially where there was a clear signal showing a contrast between the Ovaille deposits and the supposed top of the glacial deposits, at a depth that was within reach by drilling. Provisions had to be made for this operation as this location was in a S2 hydrogeological zone (inner groundwater protection zone for drinking water requiring special permitting), which implied a multi-step authorization request and procedure with the Canton of Vaud's hydrogeological as well as forest services, and the Municipality of Corbeyrier. Based on the scientific relevance of the borehole, an exception was granted to drill at the targeted point under the following provisions: (1) no fluids

could be injected during the operations (dry drilling), (2) obligation to sample the nearby water uptake source before and after drilling, (3) producing a hydrogeological report, (4) filling the borehole with the in situ material at its bottom and clay pellets in the top 4 m to avoid a preferential zone of surface water infiltration, (5) numerous environmental and safety matters such as using a tarpaulin under the drilling equipment, biodegradable oils and, generally, high standards to protect nature. All these conditions have been met.

The borehole was drilled vertically to a depth of 10.6 m, first with a 140 mm diameter bit to a depth of 3.15 m, followed by a diameter of 116 mm for the rest of the hole. The cores were retrieved by the drilling team and laid into core boxes in their original structural context as much as it was possible to do considering the nature of the rocks. The cores were first described on-site by visual inspection and photos were taken in the "fresh" condition (Fig. 2). Later, after transportation to the University of Lausanne, they were described in great detail, by visual inspection and by manipulative tests to distinguish material texture (clay vs. silt), and by applying the classification codes in Naef et al. (2019). The core is stored at the University of Lausanne and is available for scientific purposes.

Fig. 2 Photos of drilled cores taken on site directly after drilling, in their fresh state. Each core box slot is 1 m long, and core sections follow one another left to right then top to bottom

3 Results

3.1 HVSR

The HVSR curves were grouped, based on iterative visual inspection by three independent observers, into 8 categories of similar patterns which are described and illustrated in Table 1. The examples in Table 1 show the HVSR curves calculated in each window of the time series along with the mean of those curves and a pick for resonance frequency, f_R.

Considering the measurements within the Ovaille, the HVSR curves reveal a predominance of sites with low resonance frequencies ($f_R < 4$ Hz) in Plan Flacon, while intermediate frequencies (6–10 Hz) are observed just below in the loose debris or scree slope region (Fig. 3). The curves with multiple peaks are limited to three points in Plan Falcon, showing low or intermediate resonance frequencies followed by either an intermediate or high peak (> 12 Hz). Further downslope, the region is characterized by the absence of distinct peaks, followed by a scattered occurrence of intermediate and high resonance frequencies. Additionally, a cluster of lower resonance frequencies appears in the southeastern part of the Ovaille. The measurements outside the Ovaille in general show no clear peak, except for two locations (one at the geologically mapped limit of the Ovaille and the other on a slope east of Plan Falcon) both exhibiting intermediate resonance frequencies. Without an appropriate velocity model, we are limited in our calculation of thickness from these frequencies, nevertheless we were able to estimate Vs values in Plan Falcon which we then used to give first order approximations of thickness of the Ovaille deposits there (see Sect. 4).

In terms of amplitudes (A_R), the values for the clear, broad and multiple peaks always exceed 2, aligning with the SESAME Project (2004) criteria for a clear peak. Nearly all amplitudes fall within a 2 to 6 range, with one peak reaching 9.7 (Fig. 3). For the curves with no distinct peak in the Ovaille, amplitudes generally range between 2 and 4, except for one outlier measurement. Outside the Ovaille, half of the measurements without a peak exhibit amplitudes between 2 and 4, while the other half fall below 2. Overall, there is no significant amplification, though, as previously mentioned, the

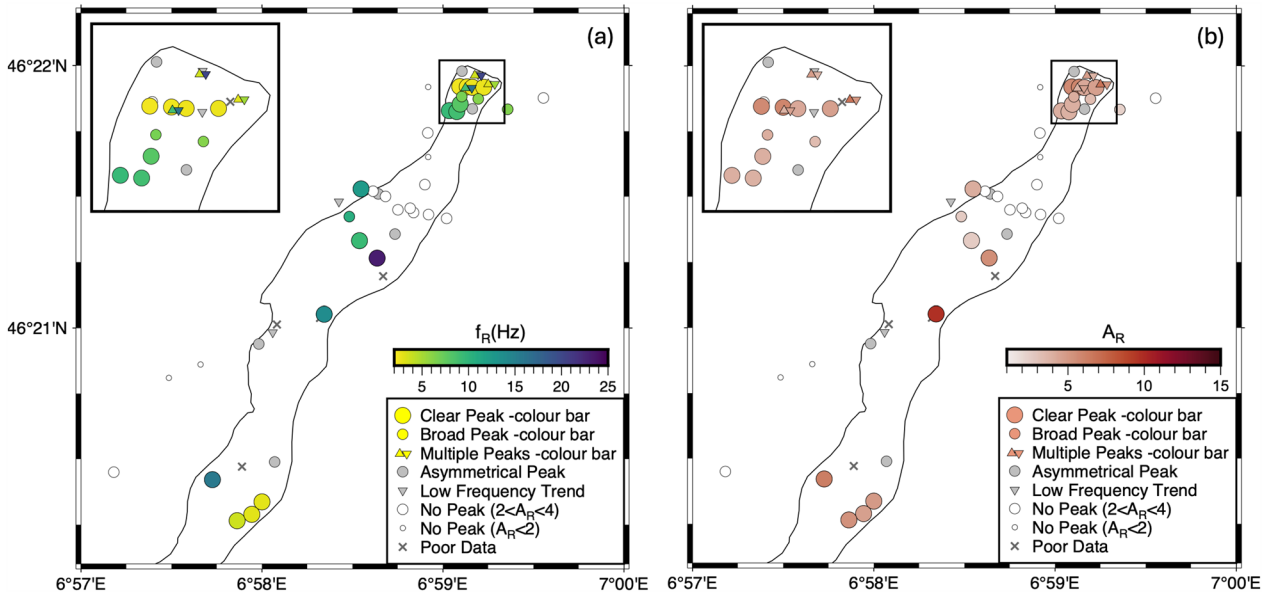

Fig. 3 **a** Distribution of the resonance frequencies f_R from the HVSR results. The colour bar represents the resonance frequencies for the clear, broad and multiple peaks categories. The trace of the Ovaille is outlined in black. The inset figure in the top left corner is zoomed into the Plan Falcon region. **b** Same as **a** but for the resonance peak amplitude A_R

HVSR method provides only a lower bound estimate of seismic amplification.

An important factor to consider in HVSR analysis is the potential influence of topographic slopes on spectral ratios. Steep terrain can alter the propagation of surface waves, potentially disrupting their development and affecting the decomposition of the wavefield into horizontal and vertical components (e.g., Tessmer et al., 1992). In sloping areas, part of the horizontal motion is projected onto the vertical axis (and vice versa), leading to a smearing effect in the HVSR curves. These effects are not yet fully understood, particularly in the context of HVSR inversion, where assumptions about the ambient seismic wavefield and forward modelling typically rely on a flat surface (e.g., Poggi et al., 2012; Molnar et al., 2018). While slope-induced effects may contribute to local variability, our analysis primarily focuses on resonance frequencies and relative amplification, rather than detailed inversion. We do not observe any correlation between local slope inclination and fundamental resonance frequency in our dataset, suggesting that topographic effects are either negligible or within the uncertainty of our measurements. Thus, for the scope of this study, we consider their impact to be secondary and do not explicitly account for them in our interpretation.

3.2 ERT and GPR

Figures 4 and 5 present the ERT and GPR results for the Luan forest profiles, respectively. For the ERT1 profile, the Wenner-Schlumberger and dipole–dipole inversion results are consistent with each other, showing a more resistive layer having a thickness of about 3.5–4 m sandwiched between a less resistive surface layer (< 1 m thick) and the sediments below. Comparing these results with the results from GPR1 where ERT1 overlaps between 150 and 250 m distance (Fig. 5), there appears to be a weak reflection around 4 m depth, which separates an upper region characterized by more chaotic scattering, and a lower region having weaker amplitudes. This change in character is somewhat less clearly seen in GPR2, and even more weakly seen in GPR3, particularly near the middle of the profile.

The ERT2 profile at Plan Falcon (Fig. 6) shows some differences compared to ERT1 in that the upper low-resistivity layer is much thicker (with an average thickness of about 5 m). This overlies more resistive sediments, which extend beyond the depth range of the resolved area (> 10 m thickness). Examining the GPR results acquired along the same profile (GPR4), this near-surface low-resistivity layer seems to correspond with an attenuation of the signal with the effect diminishing to the south (Fig. 7). This effect is also seen in GPR5 and to a lesser extent in GPR7. The results from GPR6 are even less coherent and while being cautious to not over-interpret, there seems to be some attenuation in the upper part of the section.

Table 1 Classification of the HVSR curves used in this study

HVSR f_R CATEGORY	DESCRIPTION	EXAMPLE
Clear peak	A distinct and well-defined peak with a frequency range <2.5 Hz	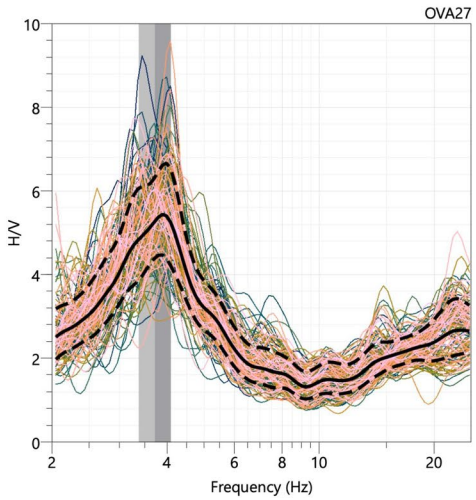
Broad peak	A peak spanning a wider frequency range (5-8 Hz), with a less well-defined maximum frequency	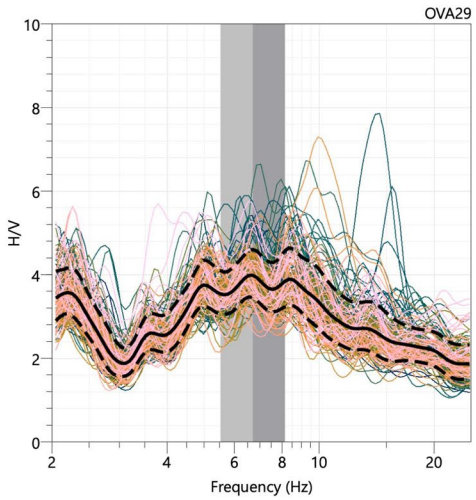
Multiple peaks	The presence of at least one clear peak accompanied by additional peaks at different frequencies	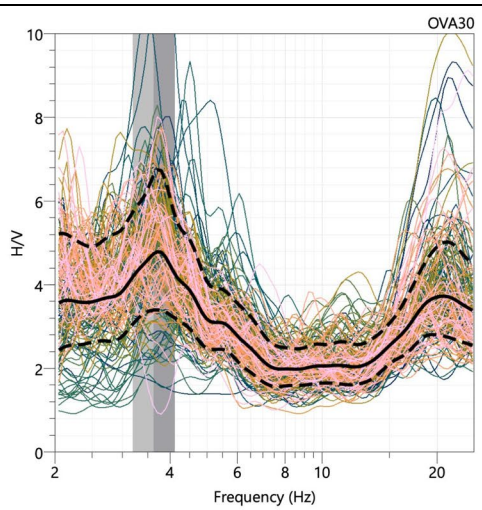

Table 1 (continued)

Asymmetrical peak	A peak with an amplitude below 4, exhibiting an irregular or skewed shape	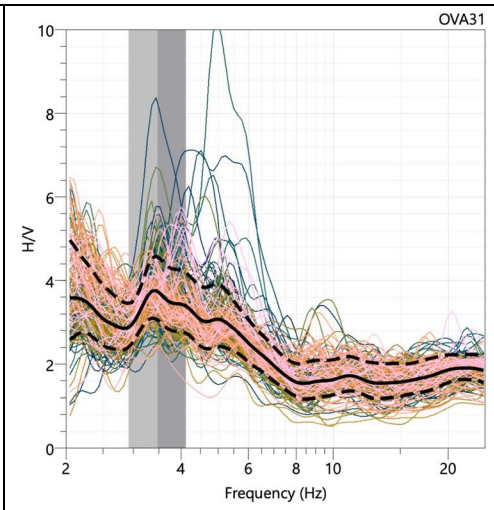
Low-frequency trend	A gradual increase in spectral amplitude toward lower frequencies without a distinct peak	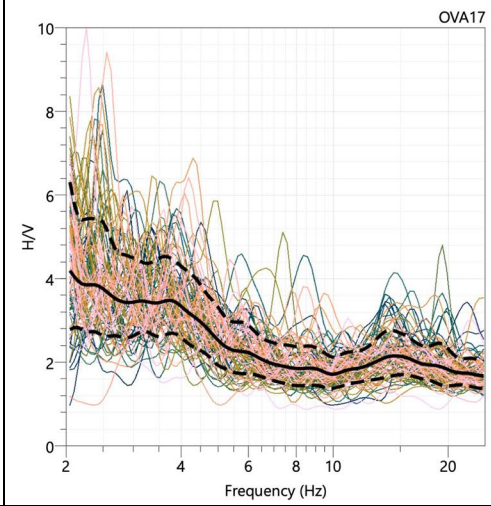
No peak (moderate amplitude)	The absence of a clear peak, with spectral amplitudes ranging between 2 and 4	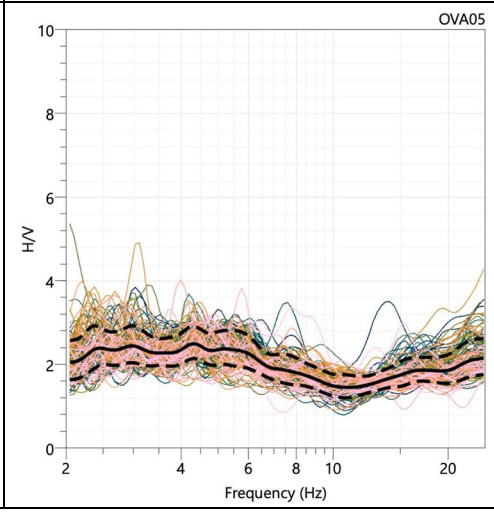

Table 1 (continued)

No peak (low amplitude)	The absence of a clear peak, with spectral amplitudes below 2	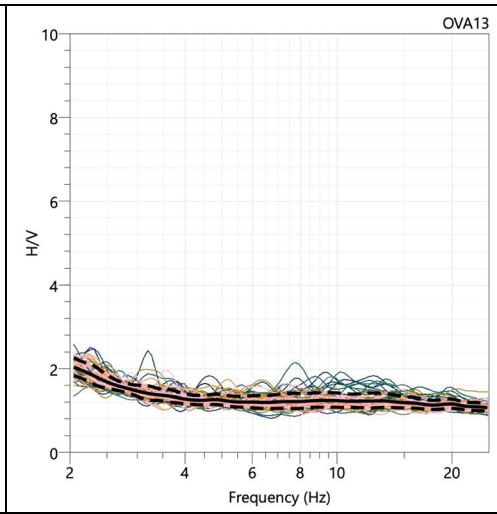
Poor data	A large spread in the standard deviation or the windowed curves are not fully coherent with each other	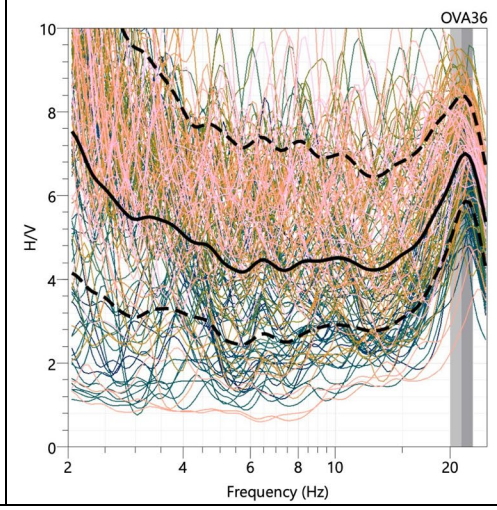

In the examples the coloured lines represent individual HVSR curves calculated in shorter windows along the time series. The solid black line represents the average of these curves with the standard deviation shown by the dashed black lines. The grey area represents the standard deviation of the peak frequency which is the value at the boundary of the light and dark grey

3.3 Drill core

The core recovered by drilling (Fig. 2) features two layers between which there is a water saturated zone that is most likely the water table (Fig. 8). The upper layer (0–3.5 m), which we classify as the Ovaille material, is an unconsolidated brecciated deposit in a clay matrix (~ 30% clay content) with angular clasts (gravel and cobbles). The bottom layer (3.5–10.6 m) is a similar brecciated deposit, but it is more consolidated with greater amounts of clay (~ 40%). We classify this layer as glacial deposits. If we extrapolate the geologic map (Badoux et al., 1960) we can possibly expect deposits of the Rhône glacier ("dépôt glaciaire rhodanien") at this location. However, the beige colour and high permeability of the material suggests that these glacial deposits are more consistent with local glacial deposits (J.F. Brodbeck, personal communication, 2024). The Rhône glacial deposits are typically grey-blue in colour and are more compacted due the weight of the glacier. In addition, these deposits share similar characteristics with the Ovaille material providing more evidence in support that the Ovaille reworked local glacial deposits. The exact limit between the two layers lies somewhere between 3.35 and 3.54 m depth, the only portion where core recovery was not complete, due to the water percolation through this depth range. This matches the depth at the nearby artificial catchment where water is taken from approximately 4 m depth.

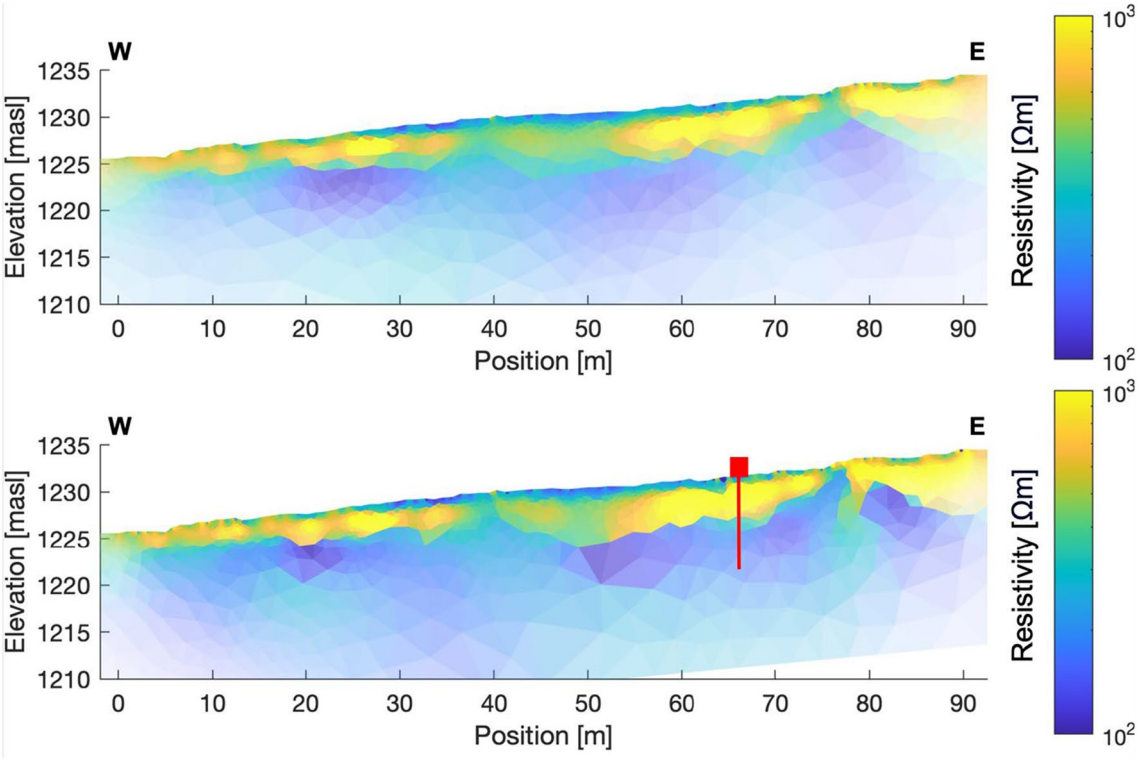

Fig. 4 Inversion results from the ERT survey in the Luan forest (ERT1), with the top panel showing the Wenner-Schlumberger survey and the bottom panel showing the dipole–dipole survey. Colours represent electrical resistivity as indicated in the colour bar. The location and depth extent of the drillhole is shown by the red square and line. Horizontal and vertical scales are alike

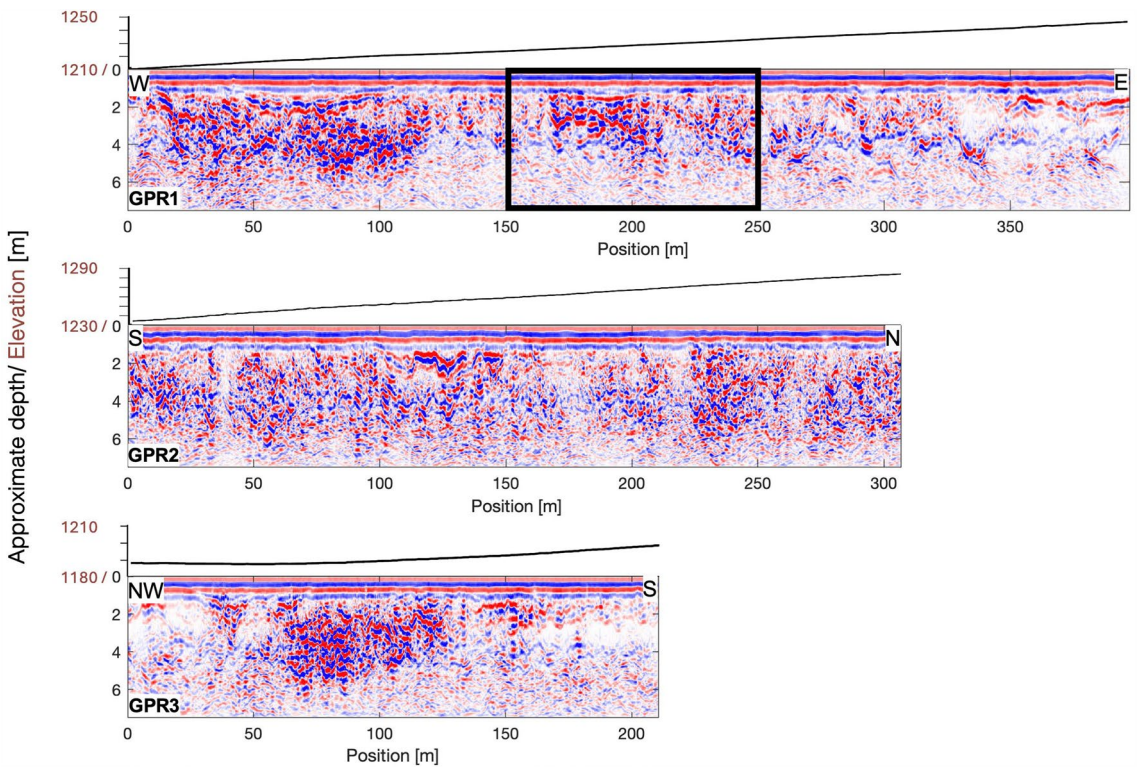

Fig. 5 GPR results for the Luan forest profiles. The black box locates the extent of ERT1 profile along the GPR1 profile. The profiles are migrated, and depths have been approximated using an assumed velocity of 0.1 m/ns. Note the various horizontal profile lengths for the same vertical scale. Elevation is plotted above each profile

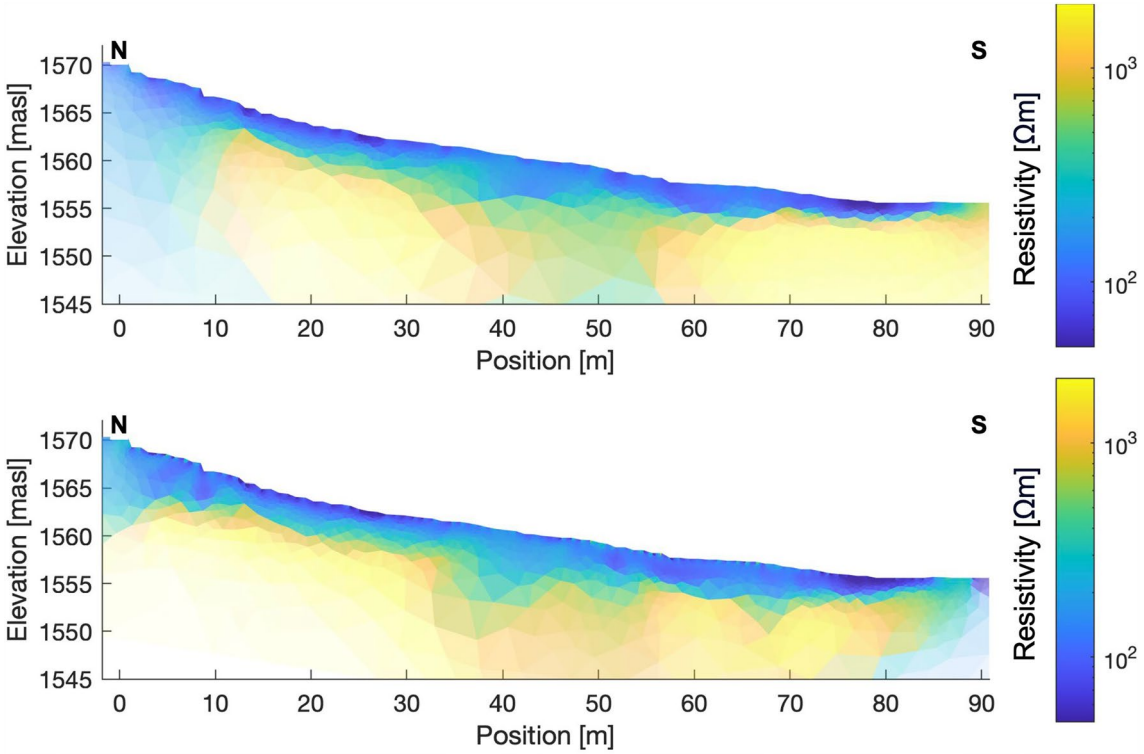

Fig. 6 Inversion results from the ERT survey in Plan Falcon (ERT2), with the top panel showing the Wenner–Schlumberger survey and the bottom panel showing the dipole–dipole survey. Colours represent electrical resistivity as indicated in the colour bar. Horizontal and vertical scales are alike

A detailed core description can be found in the Supplementary Information.

4 Discussion

The distribution of the peaks of the HVSR curves reveals the presence of two distinct impedance contrasts: a deeper interface, generating the low frequency peak, in the region of Plan Falcon, and a shallower interface, responsible for the development of the higher frequency peaks, downslope (Fig. 3). This is supported by the ERT results that depict a more electrically resistive layer with a thickness of 3.5–4 m in the Luan forest (ERT1), that appears significantly thicker in Plan Falcon (ERT2). We interpret this layer as the Ovaille deposits which is corroborated by the core drilled in the Luan forest. The drill core also confirmed that the thin near-surface low resistivity layer observed here was due to weathered deposits. Underlying the Ovaille layer, the ERT results from the Luan forest show a decrease in resistivity, which can be attributed to the increased clay content in the glacial deposits. The increased clay content could also be the reason why the GPR signal in this region is attenuated. Moreover, the presence of the water table could enhance this effect, as saturated material would also increase conductivity and attenuation of the GPR signal. Thus, the changes seen in the ERT and GPR signals could represent both the transition from unsaturated to saturated sediments and the change in sediment composition (e.g. Everett, 2013), which point to the transition from the Ovaille material to glacial material. The HVSR in this area of the Luan forest showed "no peak" with amplitudes between 2 and 4 (Fig. 3). This could be due to the absence of a strong impedance contrast within that frequency range, as seen in the drill core, where the glacial material and Ovaille material appear fairly similar, with clay content being the primary distinguishing factor. Conversely, regions with a flat HVSR with A_R around 1 are typically associated with hard rock or homogeneous, very stiff sediments, which do not significantly alter the ground motion ratio between horizontal and vertical components (e.g., Haghshenas et al., 2008; Xu & Wang 2021). This is consistent with measurements taken on bedrock outside of the Ovaille (Fig. 3—No Peak $A_R < 2$) and at one location within the Ovaille where the deposits have been excavated by humans. Further downslope, the presence of higher-frequency peaks is likely attributed to local variations occurring over a scale of a few metres. A cluster of lower-frequency well-defined peaks is also observed in the southeastern part of the Ovaille. This may be attributed to the mixing or reworking of materials, leading to

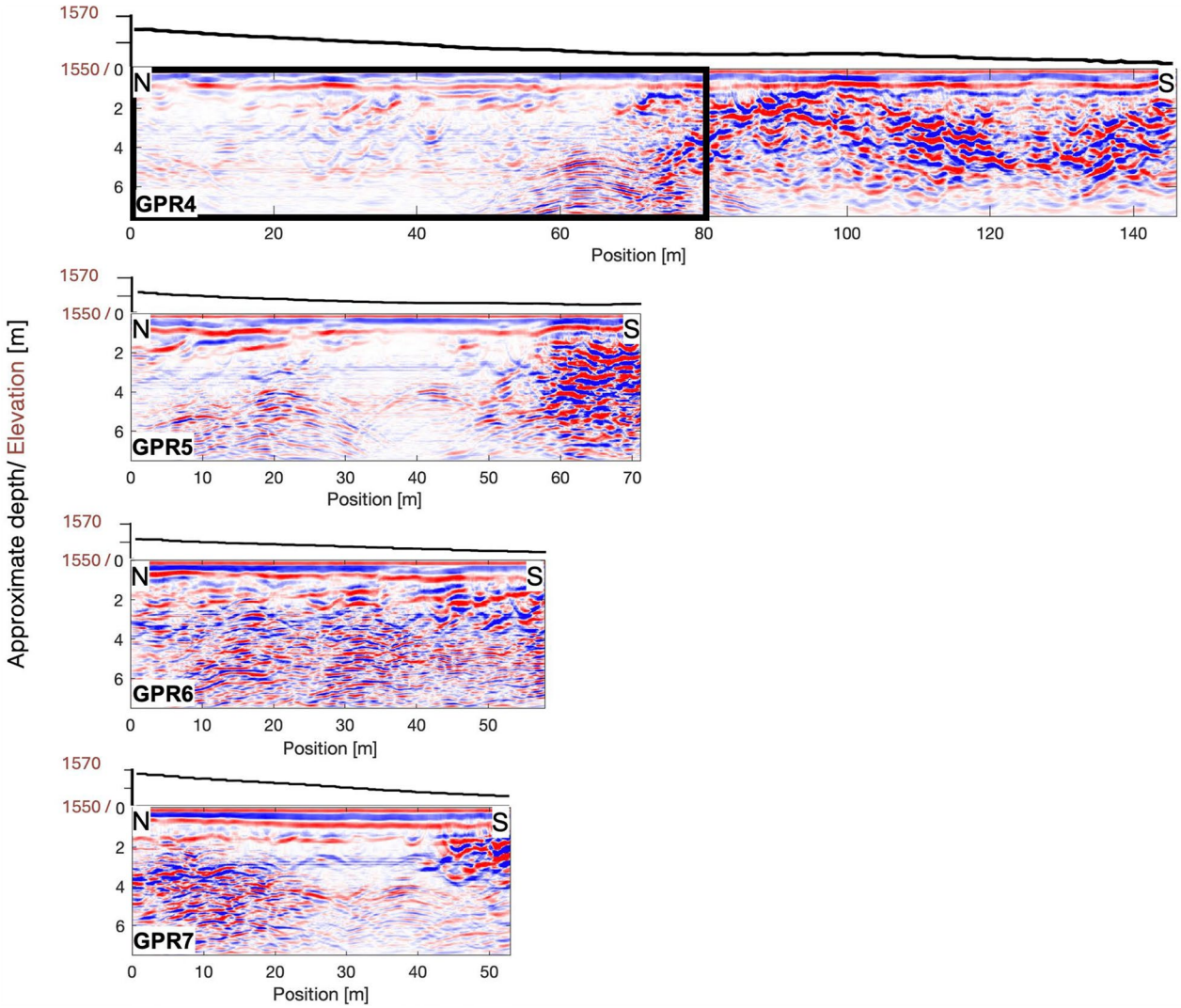

Fig. 7 GPR results for the Plan Falcon profiles. The black box shows the extent of the ERT2 profile along the GPR4 profile. The profiles are migrated, and depths have been approximated using an assumed velocity of 0.1 m/ns. Note the various horizontal profile lengths for the same vertical scale. Elevation is plotted above each profile

a reduced impedance contrast between the Ovaille and glacial deposits and sharper impedance contrast with the underlying rock. Alternatively, these peaks could result from the local remobilization of deposits due to erosional processes.

In Plan Falcon the more electrically resistive Ovaille material shown in ERT2 reaches a thickness greater than 10–15 m and is overlain by a less resistive layer that attenuates the GPR signal. We interpret the latter as surface run off deposits with greater clay content as this area is just below the landslide scarp. The presence of the multiple peaks of the HVSR may be indicative of multiple impedance contrasts and could be showing a shallow contrast possibly between the surface run-off and Ovaille material (higher frequency range) and a deeper contrast possibly between the Ovaille material and glacial deposits (lower frequency range). On the other hand, the multiple peaks may be a result of higher-mode interactions in the surface wavefield, however, determining this would require inversion modelling, which is beyond the scope of this study. Broad peaks are also observed in this region, which may indicate spatial heterogeneity in the subsurface or lateral variabilities. Alternatively, they could reflect a gradual impedance transition rather than a sharp contrast between deposits (e.g., SESAME Project, 2004). The Ovaille deposits are too thick to be resolved with the limited aperture ERT profile and the limited depth-penetration GPR profiles, and surveying much longer segments is greatly hampered by the terrain conditions.

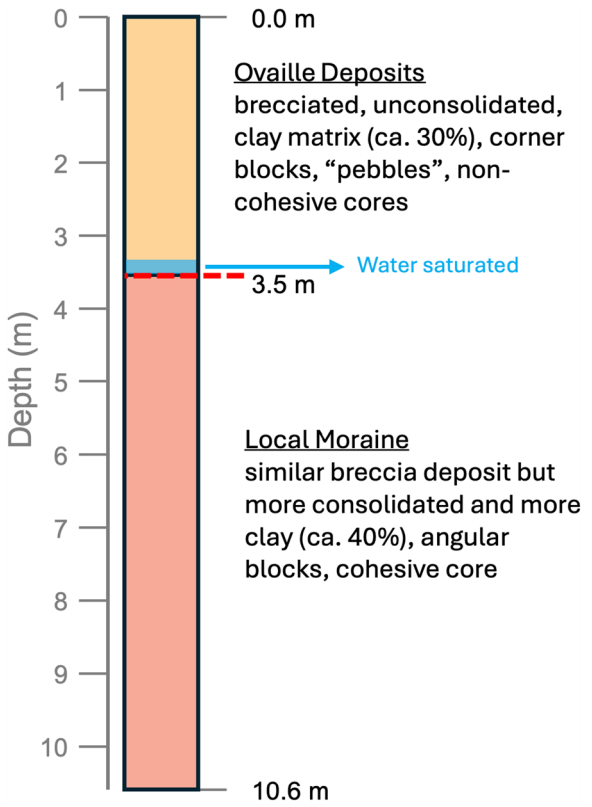

Fig. 8 Simplified core log. A more detailed log can be found in the Supplementary Information

A realistic estimate of the thickness and volume of the Ovaille material under Plan Falcon could be made by interpolating the topography of the slopes adjacent to the Ovaille, defining it as the base of sliding, and then calculating the volume above this reference surface. Since the geometry of this base is subject to uncertainties, we estimate the thickness in a simplified manner, by comparing topographic profiles along four segments (Fig. 9). The topographic relief at the southern edge of Plan Falcon is at least 50 m compared to neighbouring segments, and up to 100 m depending on the reference elevation chosen to match the profiles and/or if one considers that the surface along segment 2 has already undergone movements in the past, which is not unlikely based on the LiDAR image (Fig. 9). This 50–100 m estimate of the Ovaille deposit's thickness at Plan Falcon (Fig. 10) remains a first-order, rough estimate, especially because the sliding surface can be found and created at greater depths too. However, it indicates that the amount of mobilized material just below the source of the 1584 Ovaille is not negligible on the order of a few million cubic metres. From these thicknesses, h, we can also get an estimate of average S-wave velocity of the deposits, V_s, in Plan Falcon using an approximate characteristic resonance frequency of 2.5 Hz from the HVSR curves there, f_R, and the following equation (e.g., Ibs-von Seht & Wohlenberg, 1999; Delgado et al., 2000):

$$f_R = \frac{V_s}{4h}$$

This gives a lower and upper bound estimate of V_s between 500 and 1,000 m/s, for a thickness of 50 and 100 m respectively. As these V_s values fall into a wide range of material deposits including clayed gravel and weathered rock (e.g., Jia, 2018), we consider them as realistic of the subsurface deposits at Plan Falcon. Thus, we can use them to convert the resonance frequency at each "clear" peak point in Plan Falcon to a thickness simply to represent the spatial variability in this area (Fig. 9c). This again shows a greater thickness at Plan Falcon that decreases moving down to the scree slope. It should be noted that this is a simplified equation that assumes a homogenous layer and deviations occur in more complicated environments (e.g. Poggi et al., 2012). Nevertheless, it provides a first rough assessment of depth and variability of the layer.

The HVSR can also provide some broad insights about sediment mobility on slopes in the event of an earthquake (e.g. Seitone et al., 2025). It detects impedance contrasts and indicates where stronger ground motion can be expected, typically under the assumption of a flat surface and buried topography (one-dimensional approximation). A well-defined, pronounced peak can indicate a strong impedance contrast between unconsolidated material and bedrock, and generally a higher chance of ground motion amplification. In some cases, however, such contrasts may also coincide with mechanically weaker interfaces—where materials of different stiffness are in contact—that could be more prone to mobilization under seismic loading. The trapping and resonance of seismic waves at these horizons may further increase dynamic stresses, potentially reducing their stability. While HVSR alone cannot be considered a diagnostic tool for slope failure, it can provide useful proxies for identifying subsurface conditions that may be more susceptible to mobilization during earthquakes. Taking this into consideration, we suggest that the regions of Plan Falcon and the scree slope should be investigated further as areas where there can be potential mobility of the Ovaille sediment in the event of an earthquake. For comparison, we applied a "vulnerability index" proposed by Nakamura (1996) which agreed with these results (see Supplementary Information). We emphasize that this is a preliminary assessment and a more detailed analysis is needed to add certainty to these results. Additionally, we note

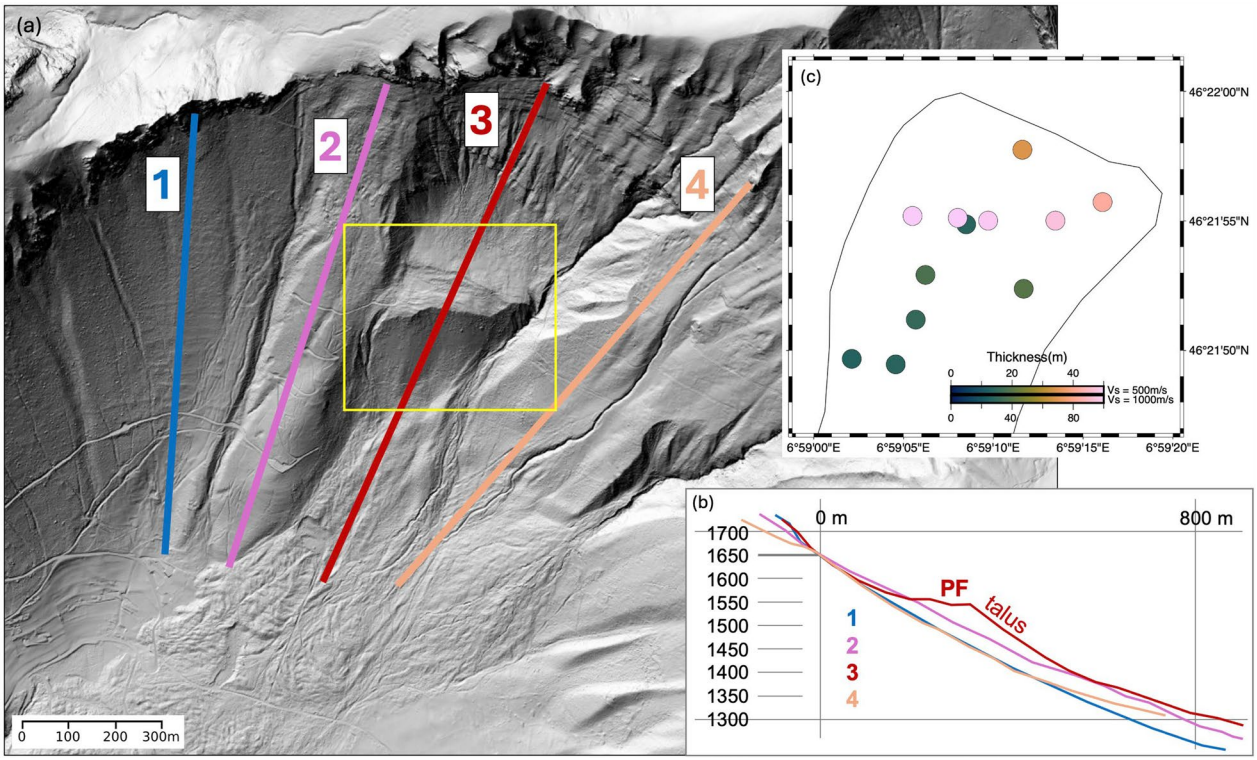

Fig. 9 **a** Topographic relief (LiDAR-based swissALTI3D monodirectional relief, from ©swisstopo) showing four profiles chosen for a first-order assessment of the lateral variation of topography, with specific interest in the relief at Plan Falcon (PF). Segment 1 is considered intact, segment 2 may have seen mass movements in the past, segment 3 is along the Ovaille and crosses Plan Falcon, and segment 4 also appears intact. Yellow box locates the region shown in (**c**). **b** Figure showing a comparison of the topographic profiles with a chosen attachment point at an elevation of 1650 m. **c** Map of re-calculated thicknesses at each point where there was a clear peak in the Plan Falcon region. The colour bar represents the thickness using the realistic bounds of Vs (500 m/s and 1000 m/s) indicating the level of uncertainty in this calculation

that the hazard of a large magnitude earthquake in this region is relatively low, and only a few houses below Plan Falcon would be vulnerable to any mass movement event, and this is made more unlikely given the stabilizing forest cover.

The ground truth obtained by the drill core is very valuable for several aspects. First, it confirms that subsurface geophysical surveying, in this case primarily ERT, provides quick and robust estimates of the physical properties and structures. The agreement between

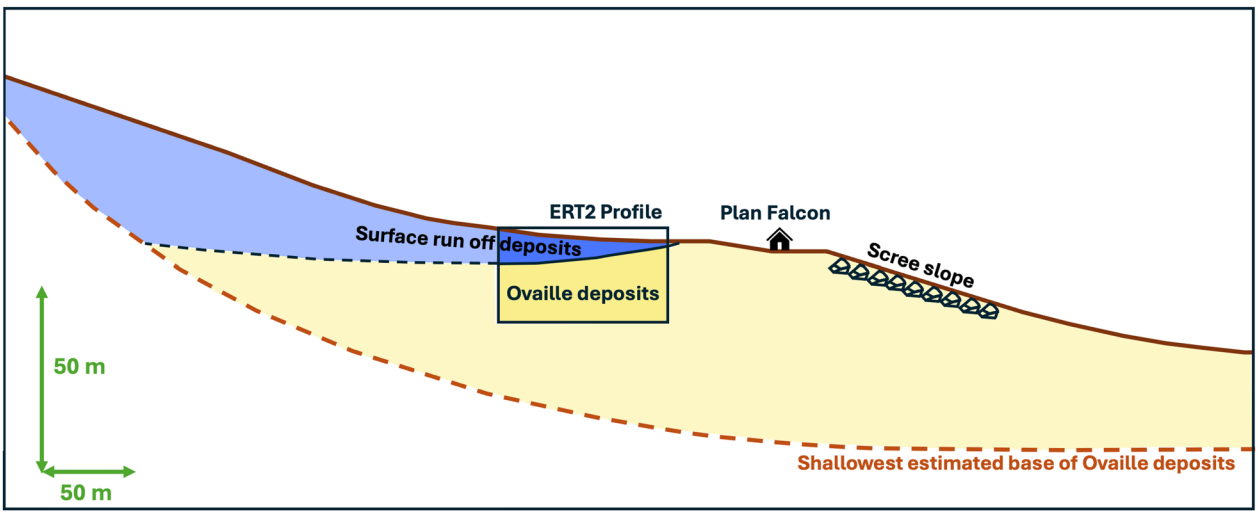

Fig. 10 Conceptual diagram of the Ovaille deposits at Plan Falcon with vertical exaggeration of 2 × horizontal

the results also allows for the interpretation of ERT data elsewhere, in terms of water and clay content variation related to changes in electrical conductivity, and possible layer thickness variations that could reflect paleo-topography. The ~ 3.5 m thickness of the Ovaille deposits also shows that the GPR images have been time-to-depth converted with approximately the right velocity (the observed contrast was at ~ 4 m depth). For the interpretation of the HVSR, the drill core provides the useful information that in the Luan forest, the physical property contrast between the Ovaille deposits and the underlying local moraine deposits are relatively small, which in turn may explain why some of the obtained HVSR amplitudes show no clear peak. Finally, from a geological point of view, the analysis of the drilled core reveals that the primary difference between the Ovaille deposits and the underlying layer is clay- (and, consequently, possibly water-) content, other than this the clasts are of similar size and nature, and correspond to the local geology uphill from the Ovaille area.

5 Conclusions

Three geophysical techniques were applied to learn about the thickness, physical properties, and ground motion effects of the 1584 Corbeyrier and Yvonne mass movement ("Ovaille") deposits. Additionally, a sediment core was drilled to give direct physical evidence and for comparison with the geophysical measurements. We measured ambient seismic noise at 54 points within and around the Ovaille to calculate the horizontal to vertical spectral ratio (HVSR). We also deployed two profiles for electrical resistivity tomography (ERT) and seven profiles for ground-penetrating radar (GPR). These measurements also show that overall, the Ovaille deposits are thicker in the region of Plan Falcon compared to downslope, such that, there were lower resonance frequencies at Plan Falcon grading into intermediate and higher resonance frequencies downslope. This is in agreement with the two ERT profiles that depicted a thicker less conductive layer greater than 10 m at Plan Falcon, and between 3.5 and 4 m thick in the Luan forest which also gave a more chaotic signal in the GPR measurements compared to the underlying layer. The drill core confirmed that the thickness of the Ovaille deposits in the Luan forest is about 3.5 m. It also showed that the Ovaille deposits are not significantly different from the underlying local glacial deposits as they are both brecciated deposits with a clay matrix, but the Ovaille deposits are more unconsolidated and have a lower clay percentage (30% vs 40%). The HVSR measurements also gave an idea of the areas where ground motion could be amplified in the event of an earthquake. We suggest there is cause for further investigation at Plan Falcon and the scree slope just below in terms of sediment mobility. Overall, a multi-pronged, geophysical and geological approach using techniques which do not necessarily provide similar results has in this case proven to be useful in characterizing paleo-events and their trace in the subsurface, and so could be simultaneously deployed in other zones of interest.

Supplementary Information

The online version contains supplementary material available at https://doi.org/10.1186/s00015-025-00494-7.

Additional file 1.

Acknowledgements

We would like to thank the Corbeyrier municipality especially Christian Roubaty, Luka Susa (fountaineer), Laurent Fivaz (forest guard) and Jean-Marie Grillon, the drilling team (Fabrice Godard, Kevin, Nicolas Berset), and Jean-François Brodbeck for the hydrogeology report. Thank you to the Canton of Vaud administration's support, Christian Gerber, Lionel Kopp and David Giorgis. We also thank Kim Lemke and Jefter Caldeira for their help in obtaining the field measurements. We thank the associate editor Simon Löw, the reviewer Adam Booth and another anonymous reviewer "H" for their constructive comments, and the chief editor Daniel Marty for the correspondence and support related to this manuscript.

Author contributions

AM and GH conceptualised the project, performed field measurements for HVSR, ERT and GPR, and oversaw the drilling operations. AM processed the HVSR data. AM, GH and VP analysed and interpreted the HVSR curves. JI performed ERT and GPR field measurements, processing and interpretation. DK contributed majorly in obtaining the geophysical field measurements (HVSR, ERT and GPR). YF described the drill core in detail. JLE contributed to the project concept, the geological background and the overall interpretation. All authors read and approved the final manuscript.

Funding

This research was funded by the Matterhorn Grant given to Ariane Maharaj from the Faculty of Geosciences and Environment, University of Lausanne, and co-funded by the Canton of Vaud. Open access funding was also provided by the University of Lausanne.

Data Availability

The seismic recordings processed in this study are publicly available on Zenodo (https://doi.org/10.5281/zenodo.15593753) and the ERT and GPR datasets are available from James Irving on request.

Declarations

Competing interests

The authors declare no competing interests. GH is a scientific editor of the journal and had fully withdrawn himself from the review process before it began.

Received: 5 June 2025 Accepted: 7 November 2025
Published online: 09 December 2025

References

Aki, K. (1957). Space and time spectra of stationary stochastic waves, with special reference to microtremors. *Bulletin of the Earthquake Research Institute, University of Tokyo, 35*, 415–456.

Alexander, D. (1983). "God's handy-worke in wonders" - landslide dynamics and natural hazard implications of a sixteenth century disaster. *The Professional Geographer*, *35*(3), 314–323. https://doi.org/10.1111/j.0033-0124.1983.00314.x

Atakan, K., Duval, A. M., Theodulidis, N., Guillier, B., Chatelain, J. L., & Bard, P. Y. (2004, August). SESAME-Team. 2004. The H/V spectral ratio technique: experimental conditions, data processing and empirical reliability assessment. In: *Proceedings of the 13th World Conference on Earthquake Engineering, Vancouver, Canada, 1–6 August*.

Badoux, H., Chessex, R., Jeannet, A., Lugeon, M. & Rivier, F. (1960). Atlas géologique de la Suisse au 1 :25'000, feuille 1284 Monthey. Commission géologique suisse.

Badoux, H. (1965). Atlas géologique de la Suisse au 1 :25'000, feuille 1265 Montreux. Commission géologique suisse.

Bard, P. Y. (1999). Microtremor measurements: A tool for site effect estimation. *The Effects of Surface Geology on Seismic Motion, 3*, 1251–1279.

Bichler, A., Bobrowsky, P., Best, M., Douma, M., Hunter, J., Calvert, T., & Burns, R. (2004). Three-dimensional mapping of a landslide using a multi-geophysical approach: The Quesnel Forks landslide. *Landslides, 1*(1), 29–40. https://doi.org/10.1007/s10346-003-0008-7

Bonnefoy-Claudet, S., Köhler, A., Cornou, C., Wathelet, M., & Bard, P. Y. (2008). Effects of love waves on microtremor H/V ratio. *Bulletin of the Seismological Society of America, 98*(1), 288–300. https://doi.org/10.1785/012007063

Caracciolo, C. H., Slejko, D., Camassi, R., & Castelli, V. (2021). The eastern Alps earthquake of 25 January 1348: New insights from old sources. *Bulletin of Geophysics and Oceanography, 63*(3), 335–364. https://doi.org/10.4430/bgo00364

Delgado, J., Lopez Casado, C., Giner, J., Estevez, A., Cuenca, A., & Molina, S. (2000). Microtremors as a geophysical exploration tool: Applications and limitations. *Pure and Applied Geophysics, 157*, 1445–1462. https://doi.org/10.1007/PL00001128

Everett, M. E. (2013). *Near-surface applied geophysics*. Cambridge University Press.

Fritsche, S., Fäh, D., & Schwarz-Zanetti, G. (2012). Historical intensity VIII earthquakes along the Rhone valley (Valais, Switzerland): primary and secondary effects. *Swiss Journal of Geosciences*, *105*(1), 1–18.

Fritsche, S., & Fäh, D. (2009). The 1946 magnitude 6.1 earthquake in the Valais: Site-effects as contributor to the damage. *Swiss Journal of Geosciences, 102*(3), Article 423. https://doi.org/10.1007/s00015-009-1340-2

Gisler, M., Fäh, D., & Giardini, D. (2008). *Nachbeben: eine Geschichte der Erdbeben in der Schweiz*. Haupt Verlag.

Günther, T., & Rücker, C. (2019). *Boundless Electrical Resistivity Tomography BERT v2. 2–the user tutorial, LIAG Hannover, TU Berlin*. http://www.resistivity.net/download/bert-tutorial.pdf.

Empirical evaluation of microtremor H/V spectral ratio. *Bulletin of Earthquake Engineering*, *6*, 75-108. https://doi.org/10.1007/s10518-007-9058-x

Häusler, M., Glueer, F., & Fäh, D. (2025). The changing seismic site response of the Brienz/Brinzauls rock slope instability: insights from 5 years of monitoring before, during and after a partial collapse in June 2023. In *Progress in Landslide Research and Technology, Volume 3 Issue 2, 2024* (pp. 47–59). Cham: Springer Nature Switzerland. https://doi.org/10.1007/978-3-031-72736-8_4

Iannucci, R., Martino, S., Paciello, A., D'Amico, S., & Galea, P. (2020). Investigation of cliff instability at Għajn Ħadid Tower (Selmun Promontory, Malta) by integrated passive seismic techniques. *Journal of Seismology, 24*(4), 897–916. https://doi.org/10.1007/s10950-019-09898-z

Ibs-von Seht, M., & Wohlenberg, J. (1999). Microtremor measurements used to map thickness of soft sediments. *Bulletin of the Seismological Society of America, 89*(1), 250–259. https://doi.org/10.1785/BSSA0890010250

Imposa, S., Grassi, S., Fazio, F., Rannisi, G., & Cino, P. (2017). Geophysical surveys to study a landslide body (north-eastern Sicily). *Natural Hazards, 86*(Suppl 2), 327–343. https://doi.org/10.1007/s11069-016-2544-1

Jeannet, A. (1912–1918). Monographie géologique des Tours d'Aï et des régions avoisinantes (Préalpes vauses). Mat. Carte géol. Suisse. N.S. 34.

Jemec Auflič, M., Jež, J., Popit, T., Košir, A., Maček, M., Logar, J., & Verbovšek, T. (2017). The variety of landslide forms in Slovenia and its immediate NW surroundings. *Landslides, 14*(4), 1537–1546. https://doi.org/10.1007/s10346-017-0848-1

Jia, J. (2018). Dynamic and Cyclic Properties of Soils. In: Soil Dynamics and Foundation Modeling. Springer, Cham. https://doi.org/10.1007/978-3-319-40358-8_2

Lanchet C., Bard P. Y., (1995, April). Theoretical investigations on the Nakamura's technique. In *Proceedings of the 3rd international conference on recent advanced in geotechnical earthquake engineering and soil Dynamics*, in St. Louis, Missouri (Vol. II)

Lanchet, C., & Bard, P. Y. (1994). Numerical and theoretical investigations on the possibilities and limitations of Nakamura's technique. *Journal of Physics of the Earth, 42*(5), 377–397.

Loew, S., Schneider, S., Josuran, M., Figi, D., Thoeny, R., Huwiler, A., Largiadèr, A., & Naenni, C. (2025). Early warning and dynamics of compound rockslides: Lessons learnt from the Brienz/Brinzauls 2023 rockslope failure. *Landslides, 22*(2), 283–298. https://doi.org/10.1007/s10346-024-02380-z

Molnar, S., Cassidy, J. F., Castellaro, S., Cornou, C., Crow, H., Hunter, J. A., Matsushuma, S., Sánchez-Sesma, F. J., & Yong, A. (2018). Application of microtremor horizontal-to-vertical spectral ratio (MHVSR) analysis for site characterization: State of the art. *Surveys in Geophysics, 39*, 613–631. https://doi.org/10.1007/s10712-018-9464-4

Molnar, S., Sirohey, A., Assaf, J., Bard, P. Y., Castellaro, S., Cornou, C., Cox, B., Guillier, B., Hassani, B., Kawase, H., Matsushima, S., Sánchez-Sesma, F. J., & Yong, A. (2022). A review of the microtremor horizontal-to-vertical spectral ratio (MHVSR) method. *Journal of Seismology, 26*(4), 653–685. https://doi.org/10.1007/s10950-021-10062-9

Moore, J. R., Gischig, V., Amann, F., Hunziker, M., & Burjanek, J. (2012). Earthquake-triggered rock slope failures: Damage and site effects. In *Proceedings 11th International & 2nd North American Symposium on Landslides* (Vol. 1, pp. 869–875). Banff, Canada: CRC Press.

Naef, H., Büchi, M., Bläsi, H.R., Deplazes, G. & Gysi, M. (2019): Lithology Manual – Lithological description of drill cores and cuttings in Northern Switzerland. Nagra Arbeitsbericht NAB 19–11. https://nagra.ch/wp-content/uploads/2022/08/e_nab19-011.pdf

Nakamura, Y. (1989). A method for dynamic characteristics estimation of subsurface using microtremor on the ground surface. *Railway Technical Research Institute, Quarterly Reports*, *30*(1).

Nakamura, Y. (1997, November). Seismic vulnerability indices for ground and structures using microtremor. In: *World congress on railway research in Florence, Italy*.

Nakamura, Y. (2000). Clear identification of fundamental idea of Nakamura's technique and its applications. In: *Proceedings of the 12th world conference on earthquake engineering* (Vol. 2656, pp. 1–8).

Nakamura, Y. (2008) On the H/V spectrum. In: Proceedings of the 14th world conference on earthquake engineering (WCEE), Beijing.

Nakamura, Y. (1996). Real-time information systems for seismic hazards mitigation UrEDAS. *HERAS and PIC. Quarterly Report-Rtri, 37*(3), 112–127.

Nogoshi, M., & Igarashi, T. (1970). On the amplitude characteristics of microtremor (Part 1). *Journal of the Seismological Society of Japan, 23*, 281–303.

Nogoshi, M., & Igarashi, T. (1971). On the amplitude characteristics of microtremor (part 2). *Journal of the Seismological Society of Japan, 24*, 26–40.

Pazzi, V., Tanteri, L., Bicocchi, G., D'Ambrosio, M., Caselli, A., & Fanti, R. (2017). H/V measurements as an effective tool for the reliable detection of landslide slip surfaces: Case studies of Castagnola (La Spezia, Italy) and Roccalbegna (Grosseto, Italy). *Physics and Chemistry of the Earth, Parts a/b/c, 98*, 136–153. https://doi.org/10.1016/j.pce.2016.10.014

Perrone, A., Lapenna, V., & Piscitelli, S. (2014). Electrical resistivity tomography technique for landslide investigation: A review. *Earth-Science Reviews, 135*, 65–82. https://doi.org/10.1016/j.earscirev.2014.04.002

Poggi, V., Fäh, D., Burjanek, J., & Giardini, D. (2012). The use of Rayleigh-wave ellipticity for site-specific hazard assessment and microzonation: Application to the city of Lucerne, Switzerland. *Geophysical Journal International, 188*(3), 1154–1172. https://doi.org/10.1111/j.1365-246X.2011.05305.x

Raetzo, H., & Loup, B. (2016). Protection against mass movement hazards. Federal Office for the Environment (FOEN), Bern.

Sass, O., Bell, R., & Glade, T. (2008). Comparison of GPR, 2D-resistivity and traditional techniques for the subsurface exploration of the Öschingen landslide, Swabian Alb (Germany). *Geomorphology, 93*(1–2), 89–103.

Schwarz-Zanetti, G., Fäh, D., Gache, S., Kästli, P., Loizeau, J., Masciadri, V., & Zenhäusern, G. (2018). Two large earthquakes in western Switzerland in the sixteenth century: 1524 in Ardon (VS) and 1584 in Aigle (VD). *Journal of Seismology*, *22*, 439–454. https://doi.org/10.1007/s10950-017-9715-8

Seitone, F., Vergnano, A., Comina, C., Bonasera, M., & Fubelli, G. (2025). Comparative analysis of geological and seismic microtremors models of a large translational landslide: The case of San Vito Romano (Central Italy). *Engineering Geology, 347*, Article 107934. https://doi.org/10.1016/j.enggeo.2025.107934

SESAME Project. (2004). Guidelines for the implementation of the H/V spectral ratio technique on ambient vibrations measurements, processing and interpretation.

Stolt, R. H. (1978). Migration by fourier transform. *Geophysics, 43*(1), 23–48. https://doi.org/10.1190/1.1440826

Tessmer, E., Kosloff, D., & Behle, A. (1992). Elastic wave propagation simulation in the presence of surface topography. *Geophysical Journal International, 108*(2), 621–632. https://doi.org/10.1111/j.1365-246X.1992.tb04641.x

Wathelet, M., Chatelain, J. L., Cornou, C., Giulio, G. D., Guillier, B., Ohrnberger, M., & Savvaidis, A. (2020). Geopsy: A user-friendly open-source tool set for ambient vibration processing. *Seismological Research Letters, 91*(3), 1878–1889. https://doi.org/10.1785/0220190360

Xu, R., & Wang, L. (2021). The horizontal-to-vertical spectral ratio and its applications. *EURASIP Journal on Advances in Signal Processing, 2021*, 1–10. https://doi.org/10.1186/s13634-021-00765-z

Publisher's Note